Time-dependent pattern formation for convection in two layers of immiscible liquids

Y. Y. Renardy and C. G. Stoltz

Department of Mathematics, 460 McBryde Hall, Virginia Polytechnic Institute and State University, Blacksburg, VA 24061-0123, U.S.A.

(March 10, 1999)

Abstract

A linear and weakly nonlinear stability analysis is performed for specific two-layer systems which have been examined experimentally in Degen et al (Phys Rev E 57, 6647 (1998)). For their water/silicone oil system, at the depth fraction where oscillations are predicted, many wavelengths are unstable. The neutral stability curve is rather flat in this region, and oscillations begin slightly above the critical Rayleigh number. The neutral stability curves for their Fluorinert/silicone oil system show that oscillations are theoretically predicted in a very narrow parameter range. A 3D Hopf bifurcation on a hexagonal lattice is investigated for patterns that arise in extended domains. In both fluid systems, travelling rolls, wavy rolls of type 1, and oscillating triangles are stable for most regimes.

47.20.Bp, 40.20.Ky, 47.54.+r.

I. INTRODUCTION

Two-layer systems heated from below have been investigated experimentally in [1]. Time-periodic oscillations were observed in rectangular and annular channels. The presence of the interface and the coupling between the fluids has generated interest in this problem from both experimentalists and theoreticians [2–6].

Figure 1 is a sketch of the system geometry. In our theoretical treatment, the system is unbounded in the horizontal directions. Distance is nondimensionalized with respect to plate separation l^*, and time with l^{*2}/κ_1 where κ_1 is the thermal diffusivity of the lower liquid. The average value of the interface height is denoted l_1. At the temperature of the top plate, each fluid has coefficient of cubical expansion $\hat{\alpha}_i$, thermal diffusivity κ_i, thermal conductivity k_i, viscosity μ_i, density ρ_i, and kinematic viscosity $\nu_i = \mu_i/\rho_i$. In each fluid, the governing equations are the heat transport equation and the Navier-Stokes equations with the Oberbeck-Boussinesq approximation. At the interface, we have: the continuity of velocity, temperature, heat flux and shear stress; the jump in the normal stress is balanced by interfacial tension and curvature; and the kinematic free surface condition holds. There are six dimensionless ratios arising from the fluid properties: $m = \mu_1/\mu_2$, $r = \rho_1/\rho_2$, $\gamma = \kappa_1/\kappa_2$, $\zeta = k_1/k_2$, $\beta = \hat{\alpha}_1/\hat{\alpha}_2$, and $l_1 = l_1^*/l^*$. We define a Rayleigh number $R = g\hat{\alpha}_1\Delta T l^{*3}/(\kappa_1\nu_1)$, where g denotes gravitational acceleration, a Prandtl number $P = \nu_1/\kappa_1$, and a dimensionless interfacial tension parameter $S = S^* l^*/(\kappa_1\mu_1)$, where S^* is the dimensional interfacial tension.

The base state for the system is given by a flat interface at $z = l_1$, a zero velocity field and a temperature field which varies linearly with z in each fluid. The gradient of the temperature field depends on the depths and the thermal conductivities. Equations governing linearized perturbations proportional to $\exp(i\alpha x + \sigma t)$, and the full equations required for a bifurcation analysis are given in Chapter III of [7]. We shall apply this to our situation where oscillations are excited by a competition between the bulk motions in each fluid, with the interface remaining approximately flat [2,1,8–13]. The fluids were chosen in

[1] to satisfy two conditions. First, the effective Rayleigh numbers of the fluids must be equal. These are $R_1 = g\hat{\alpha}_1 \Delta T_1 l_1^{*3}/(\kappa_1 \nu_1)$, and $R_2 = g\hat{\alpha}_2 \Delta T_2 l_2^{*3}/(\kappa_2 \nu_2)$, $l_2^* = l^* - l_1^*$. The continuity of heat flux across the interface fixes the ratio $\Delta T_1/\Delta T_2$ to be $l_1/(\zeta l_2)$. Using this, the ratio R_1/R_2 is $(\beta r)/(\zeta m \gamma a^4)$, where $a = l_2/l_1$. When this ratio is approximately 1, an oscillatory onset is intuitively expected. This yields the depth ratio $a = [(\beta r)/(\zeta m \gamma)]^{1/4}$. However, [12] has shown that this condition alone is not sufficient for exciting time-periodic states, and a second condition required of the system is that it be sufficiently far from self-adjoint. For large Prandtl numbers and a non-deformable interface, it is shown that when $\gamma \beta r = 1$, the onset is steady. Therefore, oscillations are more likely to be found when this combination moves farther away from 1. These criteria led to the choice of two fluid pairs: a layer of Fluorinert lying below a layer of silicone oil 47v10, and silicone oil 47v2 lying over water. The properties of these fluids are given in Table I.

For the Fluorinert/silicone oil system, the effective Rayleigh numbers are balanced when the dimensionless lower liquid depth is approximately 0.43. For this system, $\gamma \beta r$ is 0.776, and steady onsets were observed [1,9]. As the temperature difference was increased in the experiments, the roll motion became irregular, and the velocity became time-dependent in the range $0.357 \leq l_1 \leq 0.382$ at a ΔT roughly 0.1^oC above the primary steady onset. The period of the time-dependent state was approximately 50 min at low ΔT. The wavelength of the pattern was found to be roughly 14.7 mm, or dimensionless wave number $\alpha = 5.2$. Linear theory predicts that Hopf modes (time-periodic oscillations) occur at dimensionless lower liquid depth 0.43, but not in the range of depths mentioned above where oscillations were observed. This shift in the depth from 0.43 to roughly 0.36 may be due to the finite geometry of the experiments, namely the width of the apparatus. In addition, the thermal and mechanical fluid properties, which were provided by the fluid manufacturers, need to be verified under laboratory conditions. Linear theory predicts that the oscillations at lower liquid depth 0.43 have periods of 50 minutes or longer, reminiscent of the periods in the experiments. The weakly nonlinear theory predicts saturation in the form of traveling rolls [12].

Since oscillations were not observed at onset for the Fluorinert/silicone oil system, a search was conducted for another fluid pair, for which oscillations would occur over a wider range of liquid depths. The guiding quantity was to make $\gamma\beta r$ as far away from 1 as possible. This led to the choice of the water/silicone oil system [17]. The linear theory in this paper details this fluid pair, for which the experimental data were more recently investigated. Time-dependent onsets were indeed observed experimentally for the depths predicted by linear theory (see Section II). However, the periods and wave numbers do not correspond.

While the experimental observation of oscillations over a wide range of lower liquid depths may appear to indicate that the water/silicone oil system is a superior pairing for examination, the choice of fluid pair is complicated by the difficulty in measuring and observing the system. The advantage of the Fluorinert/silicone oil system and the disadvantage of the water/silicone oil system are discussed in [1].

II. LINEAR STABILITY

A. The water/silicone oil 47v2 system

We examine the linear stability to two-dimensional disturbances with wave number α in the x-direction and dependence on time through $\exp(\sigma t)$. The equations governing this system and numerical techniques used here are given in Chapter 3 of [7]. For the water/silicone oil 47v2 system, interfacial tension was estimated using Antonow's rule [17]: $S^* = 71.2 - 18.7 = 52.5$ dyn/cm. The parameters for this system are $P = 7.1, r = 1.149, m = 0.576, \beta = 0.1766, \zeta = 5.44, \gamma = 1.845$. Balancing the Rayleigh numbers yields $l_1 = 0.7$, and $\gamma\beta r = 0.374$. With plate separation $l^* = 1.29$ cm, $G = (RP)/(\hat{\alpha}_1 \Delta T) = 1.04 \times 10^9$. The dimensional period is $2\pi l^{*2}/(\mathrm{Im}\sigma\kappa_1)$. The dimensional wavelength is $2\pi l^*/\alpha$. Figure 2 shows the relationship between the dimensionless variables and dimensional quantities for the rectangular channel in the experiments of [1]. Figure 20 of [1] shows the temperature differences at depths 0.60, 0.67 and 0.71 for oscillatory onsets to be 0.62 ^oC, 0.68 ^oC, and 0.70^oC,

respectively, and these conditions are above the theoretically predicted criticality. Figure 2 shows the conversion of physical quantities to dimensionless parameters.

Figure 22 of [1] shows the periods and wave numbers observed in the top layer, for lower liquid depth $l_1 = 0.71$: wave lengths of 7 mm ($\alpha = 11.6$), and periods of roughly 23-30 minutes ($\mathrm{Im}\sigma = 3.5 - 4.6$). These data were taken for temperature differences of 0.8^oC to 1.6^oC [17].

1. Neutral Stability Curves

Figure 3 shows the trends in the critical Rayleigh number vs wave number, and figure 4 shows the $\mathrm{Im}\sigma$ vs wave number, for dimensionless lower fluid depths $l_1 = 0.62$ to 0.71. For the depths illustrated in figure 4, the neutral stability curves show possible time-periodic states in the range of wave numbers roughly 2 to 6. At each depth in figure 3, the trough of the Rayleigh number vs wave number plot yields the onset mode. The lowest points of the troughs belong to steady modes. However, the trough is rather flat over many wave numbers, and the tendency from depth 0.6 to 0.69 is that a wave number larger than 5 is the onset mode, while there is a switch at depth 0.7, and the wave number less than 5 becomes the onset mode. Looking at the neutral stability curves, this switch occurs because the curve develops two lobes in the presence of the Hopf modes, with one lobe descending and the other rising. The depth ratio 0.7 is unique in that the troughs of the neutral stability curve hit two wave numbers at approximately a 2:1 ratio. Not only does this complicate the dynamics, but for Rayleigh numbers just above onset, the Hopf modes are also excited. Furthermore, the wave number, which is twice that of the Hopf mode, is also unstable at roughly the same Rayleigh number with a steady mode. Thus, especially at $l_1 = 0.7$ where experimental data were taken, we would expect to see resonances and complicated dynamics over many wave numbers. At the other depth ratios, the onset mode is steady, but the Hopf modes exist at Rayleigh numbers very close to that of the onset mode. The critical Rayleigh numbers and wavenumbers are shown in Figure 5: for each depth l_1, the critical mode is found from the

neutral stability diagrams by finding the lowest Rayleigh number and corresponding critical wave number.

Hopf modes are evident for dimensionless lower liquid depths 0.62 through 0.7. The shortest periods are around 26 minutes (Im$\sigma = 4$) at $l_1 = 0.66$ and wavelength 22 mm (wave number 3.5). The period at $l_1 = 0.7$ and wavelength 13mm (wave number 5.7) is 70 minutes (Im$\sigma = 1.5$). Measurements reported in [1] at depth fraction 0.71 are shown in their Figures 21 and 22. They show plots of period vs ΔT and wave number vs ΔT for ΔT from roughly 0.7 to 2 ^oC. The lowest value of ΔT which they record corresponds to Rayleigh numbers just above 20,000 (see Figure 2) and we see from our neutral stability curve in Figure 3 that for a Rayleigh number of 20,000, many wave numbers are already unstable. Experimental data in Figure 20 of [1] show the critical values of ΔT at lower liquid depths 0.6, 0.67 and 0.71 which give Rayleigh numbers 19,000, 20,800 and 21,500, respectively. Comparing with the neutral stability curves in Figures 3- 4, we would expect to see the oscillations induced at lower liquid depths 0.67 and 0.71. The available data concerning the oscillations are shown in their Figure 21 for depth 0.71, which plots the primary oscillation period and primary wave numbers. We need more information than currently available, such as graphs of the power spectral density for their signals or some form of Fourier Transform of their observed periods, to interpret the experiments in light of the theory. Such graphs would show more clearly the relative strengths of the periods that are observed. Our interpretation of the data given for depth 0.71 is that at the Rayleigh number of 21,500, it is possible for the recorded wave number around 11, corresponding to a trough of the neutral stability curve, to be unstable, as well as its subharmonic at wave number 5.5, which is close to a time-periodic mode. If the lower liquid depth were .01 or .02 less, then there would be a resonance of the steady mode at wave number 11 with a subharmonic mode at wave number 5.5 which is time periodic with the period lying in the range shown in Figure 22 of [1]. There is some scatter in their Figure 22 and periods range from 15 to 40 minutes.

The onset mode at each depth fraction is shown in Figure 5 and all are steady. However, when the Rayleigh number is increased slightly above onset, especially around $l_1 = 0.7$, the

Hopf modes become unstable as well. However, if it is increased further, the Hopf modes can split into two real modes. The two branches of real modes are illustrated for depth fraction 0.69 in Figure 6 at R=18,822.71, for $\Delta T = 0.62^o$C, and R=19,733.49 for $\Delta T = 0.65^o$C.

Around $l_1 = 0.69$, the critical Rayleigh number is almost independent of wave number over a wide range of wave numbers, complicating a full theoretical analysis. Time-periodic oscillations around wave number 5 to 6, and steady modes around wave number 4, as well as from 10 to 11, are unstable under experimental conditions. When the Rayleigh number is pushed above onset, the fastest growing modes are those at wave numbers 10 to 11, as evident from Figure 6. At $l_1 = 0.69$, The Imσ maximum is 2.6, yielding a period of 47 minutes. At $l_1 = 0.7$, Im$\sigma_{max} = 1.6$, giving 77 minutes.

As l_1 decreases to around 0.62, the oscillatory modes move to longer wavelengths which have much higher critical Rayleigh numbers. This is illustrated in Figure 4 where the case of depth ratio 0.63 is shown for wave numbers from 2. The experimental device has a long-wave cut-off due to the limited length. The rectangular device is 78 mm by 21 mm, and 78 mm corresponds to dimensionless wave number 1. Wave numbers less than 2 are not included in the neutral stability graphs.

2. Behavior of Eigenmodes

Temperature Contours We examine contours for the perturbation temperature field of the onset modes. These are the modes shown in Figure 5 for each depth fraction and all are steady. From lower liquid depths of 0.60 to 0.69, the perturbation temperature field is dominant in the top layer as shown in Figure 7(a) for lower liquid depth 0.6 and wave number 6.7. At lower liquid depths of 0.70 to 0.75, the perturbation temperature field consists of one large roll covering both layers as shown in Figure 7(b) at depth 0.7 and wave number 3.7.

At $l_1 = 0.7$, the neutral stability curve of Figure 3 shows a unique situation, where more than one wave number would in practice become unstable together. Specifically, at wave

number 3.7, the critical Rayleigh number is 12,119 while at wave number 8.9, it is 12,135. For the critical curves in Figure 5, we have chosen strictly the lowest onset Rayleigh number and corresponding wave number. Depth 0.7 also has the oscillatory modes becoming unstable at wave numbers 5.6 to 5.8, with 5.8 at Rayleigh number 14,868. According to Figure 2, these Rayleigh numbers occur for temperature variations of less than 0.5 ^oC, while experimental data were taken slightly above this. The behavior described above for depth fractions 0.70 to 0.75 can be explained by the presence of two troughs in the neutral stability curves. The trough with the higher wave numbers reveals the same behavior as was observed for the critical points for lower liquid depths from 0.60 to 0.69: the perturbation temperature field is dominant in the top layer. For example, at depth 0.7 and wave number 9, the contour plot is similar to Figure 7 (a). The only difference is that the rolls penetrate a shorter distance down because the wave length is shorter.

As evidenced by the neutral stability curves in Figure 3, depth fractions between 0.62 and 0.70 possess oscillatory onsets. For wave numbers slightly less than those of the oscillatory range, the temperature field consists of a large roll covering both layers as shown in Figure 8(a) at wave number 5.4. At the mode with the maximum Imσ, the perturbation temperature field consists of linked rolls between the two layers as shown in Figure 8(b) for wave number 5.7. Slightly above the wave number for oscillations, the perturbation temperature field consists of rolls in each fluid as shown in Figure 8(c) at wave number 6. For higher wave numbers, the roll in the top begins to dominate so that at wave number 9, the situation as in Figure 7(a) is retrieved.

The overall behavior of the perturbation temperature field has four stages as the wave number increases from steady modes, through time-periodic modes, then back to steady modes: (1) a single large roll over the entire depth as in Figure 8(a), (2) a linked roll as in Figure 8(b), (3) separate rolls in each layer as in Figure 8(c), and (4) roll in the top fluid only, as in Figure 7 (a).

Velocity Field Finally, we investigate the velocity vector fields for those depths that possess oscillatory onsets. There are three distinct patterns that emerge: thermal coupling,

mechanical coupling, and a transition state that exists as a blend of the two types of coupling. (For definitions of thermal and mechanical coupling, we refer the reader to [1,2,8,9].) For depth fractions from 0.65 to 0.70, a distinct three-step pattern is evident as the wave number increases: (1) at wave numbers less than those of the Hopf region, thermal coupling as in Figure 9(a), (2) at wave numbers in the Hopf region, transition state as in Figure 9(b), (3) at wave numbers greater than those of the Hopf region, mechanical coupling as in Figure 9(c). These results are summarized in Table II. At depth fractions 0.62 - 0.64, steps (2) and (3) from above hold true, however there are no applicable wave numbers less than those of the Hopf region. In addition, at very low wave numbers, i.e. less than one, the Rayleigh number is extremely large, on the order of 10^5, leading to questions about experimental accessibility of these results.

B. The Fluorinert/silicone oil 47v10 system

For the Fluorinert/silicone oil 47v10 system, the plate separation is 1.26 cm, $P = 406.3, \beta = 0.93, \gamma = 0.40, r = 2.09, \zeta = 0.54, m = 2.93, G = (RP)/(\hat{\alpha}_1 \Delta T) = 1.7 \times 10^{10}$. For an interfacial tension of 7 dyn/cm [16], $S = 94.2 \times 10^3$. The linear stability results change very little with change in interfacial tension (at 20 dyn/cm, the results are essentially the same). Figure 10 shows the relationship between the dimensionless variables and dimensional quantities.

The experimental measurements in Figures 3.16 and 3.17 of [17] show that at depth $l_1 = 0.375$, oscillations are recorded for $\alpha = 5.2$, with periods between 45 and 80 minutes. The experiments were performed for temperature differences ΔT of 1 to 2 ^oC. At $\Delta T = 1$ ^oC, for which the Rayleigh number is roughly 36,000. The linear theory predicts that steady modes become unstable at wave number 5.2, as shown in Figure 5.

1. Neutral Stability Curves

The critical curve in Figure 5 belongs to a steady onset mode. However, the neutral stability curves in Figures 11 and 12 illustrate that there is a small interval of wave numbers from 3.2 to 4.2 at the lower liquid depth of 0.43 which are oscillatory. This is the lower liquid depth at which Rayleigh numbers for the two layers are balanced. The window of oscillations was not detected in [12] because it is so small.

2. Behavior of Eigenmodes

Temperature Contours Eigenfunctions were examined for the perturbation to the temperature field. Perturbation temperature contour plots are shown in Figures 13 - 14. We begin by examining the critical modes (the lowest Rayleigh number for onsets as shown in Figure 11). These are steady modes. For lower liquid depths $l_1 = 0.36$ to 0.40, the roll in the upper layer is dominant, with little going on in the bottom layer, as shown in Figure 13(a) for depth 0.36. The convection in the bottom layer begins to increase as the depth fraction changes from 0.36 to 0.40. At 0.41, the perturbation temperature field in the bottom layer is noticeably larger in magnitude than at lower liquid depth fractions, as shown in Figure 13(b). A transition takes place between lower liquid depths 0.41 and 0.42, and for depths 0.42 to 0.44, the dominant temperature field of the onset mode is in the bottom layer, as shown in Figure 13(c). Since at depth 0.43, the Rayleigh numbers are matched for both layers, we expect to see rolls in both layers and oscillations. However, the onset mode at 0.43 is steady.

We next examine the oscillatory regime at depth 0.43. Oscillatory onsets occur along the neutral stability curve at $l_1 = 0.43$ for wave numbers 3.2 to 4.2, a very narrow range. For a wave number slightly less than 3.2 (see Figure 14(a) at $\alpha = 3$) the motion consists of steady rolls in the upper layer. Within the oscillatory regime, (see Figure 14(b) at $\alpha = 3.7$), contours of the perturbation temperature field are joined for both layers in the shape of

linked rolls and both liquids have equally dominant values, as expected from the balance in the Rayleigh numbers. Slightly above wave number 4.2 (see Figure 14(c) at $\alpha = 5$) the motion is dominated by steady rolls in the bottom fluid. This dominance of the bottom layer is found to still be present at wave number 6. Thus, the temperature field is dominant in one of the fluids, not both, as the oscillatory regime is approached, and the rolls then become of equal magnitude in both layers within the oscillatory regime.

Velocity Field Finally, we investigate the velocity vector fields at depth fraction 0.43. As in the water/silicone oil system, distinct patterns emerge as the wave number varies. However, unlike the water/silicone system, at wave numbers less than those of the Hopf region, the system exhibits moderate mechanical coupling, not thermal coupling, as shown in Figure 15(a). It should be noted however, that at wave numbers less than those of the Hopf region, the motion takes place almost entirely in the top layer of fluid, and so the mechanical coupling behavior may not be detectable experimentally. In the Hopf region, the system is in transition as shown in Figure 15(b), and at wave numbers greater than those of the Hopf region, mechanical coupling is once again evident, as shown in Figure 15(c).

III. HOPF BIFURCATION IN 3D

The group in [1] has on-going plans to do experiments in larger cells, and this motivated a theoretical analysis for solutions which are doubly periodic with respect to a hexagonal lattice. Other types of spatial periodicities such as square [20] or rhombic are equally worth investigating. The symmetry of the hexagonal lattice causes a sixfold degeneracy of the critical eigenvalue. Hopf bifurcations of this type have been investigated extensively [18,19,7], and we merely present results here. There are eleven qualitatively different types of bifurcating solutions: standing rolls, standing hexagons, standing regular triangles, standing patchwork quilt, travelling rolls, travelling patchwork quilt of type 1, travelling patchwork quilt of type 2, oscillating triangles, wavy rolls of type 1, wavy rolls of type 2, and twisted patchwork quilt. Table III lists the stable solutions which we found. None of the standing

wave solutions are stable. Traveling rolls, wavy rolls of type 1, and oscillating triangles appear in each system. The water/silicone oil system also exhibits the traveling patchwork quilt of type 2 for three situations, which are at the low wave number side of the Hopf range for lower liquid depths 0.62, 0.65 and 0.66. At the lower end of the depth fractions, 0.62 and 0.63 show a preference for traveling rolls. As the depth fraction increases, more exotic solutions such as the wavy rolls of type 1, and oscillating triangles also appear. At depth fraction 0.7 which is the largest depth fraction displaying a Hopf range, oscillating triangles are stable for wave numbers throughout the Hopf regime.

IV. CONCLUSION

We have investigated pattern formation in two specific systems, motivated by experimental observations of oscillations in rectangular and annular systems [1].

The first is composed of silicone oil Rhodorsil 47v2 lying over water. Experimental data in [1] were taken around depth fraction 0.6 to 0.71. Recorded periods at depth fraction 0.71 show a primary period around 25 minutes, with scatter up to 40 minutes. The primary wave number is 10 with scatter from 1 to 80. Our linearised stability analysis at depth fraction 0.7 predicts modes over many wave numbers with the strongest being (i) steady modes 4 to 5, (ii) steady modes 9 to 10, and (iii) oscillatory modes, period 50 minutes at wave number 5.4. The investigation of the temperature contour plots shows that much of the action occurs in the water layer for the oscillatory range and for the steady modes around wave number 5, but the higher wave number around 10 induces roll action in the top layer. Therefore, since experimental visualisation is difficult in the lower water layer [17], one possibility is that the horizontal scale of wave number roughly 11 was observed in the upper layer representing the steady mode, which has a wavelength half that of the oscillatory mode (Figure 22(b) of [1] records some secondary wave numbers in this range), together with a record of the oscillation period for wave number roughly 5.5 which has less going on in the upper layer than the steady mode. There is high sensitivity to the depth fraction. At depth fraction 0.69,

the period shortens to 30 minutes, and at depth 0.68 to 25 minutes. The period shortens as the depth fraction decreases to 0.65, as evident from our neutral stability curves. For this system therefore, we would suggest that controlled experiments be aimed at lower liquid depths 0.65 to 0.68 and at a specific wave number targetting the oscillatory range. Even at these depths, it is likely that a band of wave numbers are unstable together, but at least these do not suffer from two troughs in the neutral stability curves.

The second system is composed of silicone oil Rhodorsil 47v10 lying on Fluorinert. We find that oscillatory instabilities are possible, but in a much narrower range of parameters than in the silicone oil/water system. The linear stability analysis of Section II reveals a small window of oscillatory modes which may become unstable if the perturbation wavelength is suitably restricted. The experimental data of [1] recorded oscillations of roughly the same wave number and period as we predict but the depth fraction is slightly different. Also, the oscillations are not primary onsets, but rather occur above criticality. This study raises the following questions for future experimental consideration: whether the width of the experimental cell affects the critical conditions, and whether the values of the physical properties of the fluids, such as viscosity, need to be re-measured. Oscillations are predicted at a higher Rayleigh number than criticality, but if the wave number is restricted, then the oscillations would be the critical modes, just as in the water/silicone oil system. For both systems, therefore, experiments for oscillatory onsets need to be seeded for specific wave numbers.

The experimental observations of steady onset, followed by oscillations at slightly higher Rayleigh number, motivated the work of [14]. For a prescribed spatial period, there are Hopf modes next to a Takens-Bogdanov point. At that point, a double zero eigenvalue with a single eigenvector is the critical mode. The region of validity for the straightforward Hopf bifurcation analysis, assuming a non-zero frequency, shrinks for situations like this with long periods [15]. The long periods are equivalent to a small $\mathrm{Im}\sigma/(\pi^2+\alpha^2)$. Time-periodic solutions, which have been analyzed for the Hopf bifurcation case (Section III), again arise in the Takens-Bogdanov case [14], but some can now be excited as a secondary

bifurcation from steady solutions rather than as a bifurcation directly from the rest state. For the Fluorinert/silicone oil system, a temporally chaotic regime with triangular spatial symmetry is predicted. Whether these patterns would be observable in experiments remains to be investigated.

ACKNOWLEDGMENTS

This research was sponsored by the National Science Foundation under Grant No. CTS-9612308.

REFERENCES

[1] M. M. Degen, P. W. Colovas, C. D. Andereck, Phys. Rev. E. **57**, 6647 (1998).

[2] F. H. Busse and G. Sommermann, in *Advances in Multi-Fluid Flows*, edited by Y. Y. Renardy, A. V. Coward, D. Papageorgiou, and S-M. Sun, (AMS-IMS-SIAM, Philadelphia, 1996), pp. 33–41.

[3] G. Z. Gershuni and E. M. Zhukhovitskii, *Convective stability of incompressible fluids* (Keter Publ. House, Jerusalem Ltd., 1976).

[4] D. Johnson and R. Narayanan, Phys. Rev. E. **56**, 5462 (1997).

[5] D. Johnson and R. Narayanan, Phil. Trans. R. Soc. Lond. A **356**, 885 (1998).

[6] D. Johnson, R. Narayanan and P. C. Dauby, The effect of air height on the pattern formation in liquid-air bilayer convection, preprint (1998).

[7] D. D. Joseph and Y. Y. Renardy, *Fundamentals of Two-Fluid Dynamics* (Springer Verlag New York, 1993).

[8] S. Rasenat, F. H. Busse and I. Rehberg, J. Fluid Mech. **199**, 519 (1989).

[9] C. D. Andereck, P. W. Colovas, M. M. Degen, in *Advances in Multi-Fluid Flows*, edited by Y. Y. Renardy, A. V. Coward, D. Papageorgiou, and S-M. Sun (AMS-IMS-SIAM, Philadelphia, 1996), pp. 3–12.

[10] C. D. Andereck, P. W. Colovas, M. M. Degen and Y. Y. Renardy, Int. J. Eng. Sci. **36**, 1451 (1998).

[11] Y. Renardy and C. G. Stoltz, in *Pattern Formation in Continuous and Coupled Systems*, edited by M. Golubitsky, D. Luss, S. Strogatz (Springer-Verlag New York, 1999) to appear.

[12] Y. Renardy, Z. Angew. Math. Phys. **47**, 567 (1996). Errata **48**, 171 (1997).

[13] P. Colinet and J. C. Legros, Phys. Fluids **6**, 2631 (1994).

[14] Y. Y. Renardy, M. Renardy, K. Fujimura, Physica D, accepted (1998).

[15] M. Renardy, Advances in Diff. Eq. **1**, 283 (1996).

[16] C. V. Burkersroda, A. Prakash, J. N. Koster, Microgravity Q. **4**, 93 (1994).

[17] M. M. Degen, Ph.D. dissertation, The Ohio State University, 1997.

[18] M. Roberts, J. W. Swift and D. H. Wagner, AMS Contemp. Math. **56**, 283 (1986).

[19] M. Renardy and Y. Renardy, Physica D **32**, 227 (1988).

[20] W. A. Tokaruk, T. C. A. Molteno, S. W. Morris, Phys Rev. Lett. submitted (1998).

[21] K. Fujimura and Y. Renardy, Physica D **85**, 25 (1995).

FIGURES

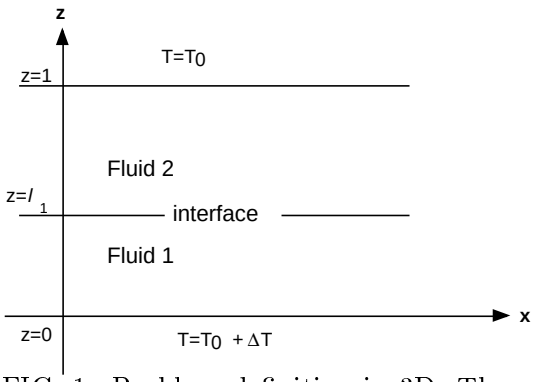

FIG. 1. Problem definition in 3D. The y-axis extends into the paper. Walls are situated at $z = 0$ with temperature $T_0 + \Delta T$ and at $z = 1$ with temperature T_0. The unperturbed interface separating fluid 1 and fluid 2 is at $z = l_1$.

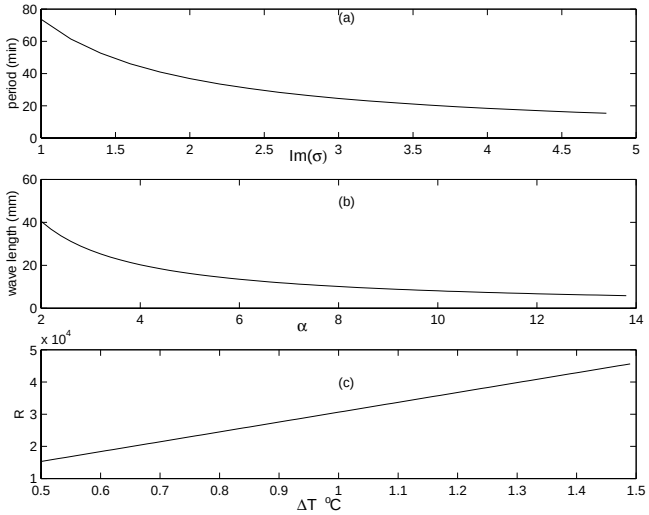

FIG. 2. Water/silicone oil system. (a) Dimensional period (min) vs Imσ. (b) Wave length (mm) vs wave number α. (c) Rayleigh number R vs temperature difference $\Delta T^o C$. Plate separation 1.29 cm.

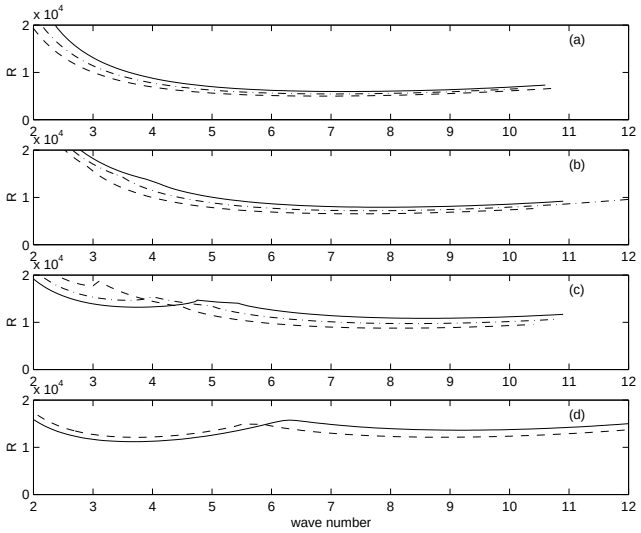

FIG. 3. Water/silicone oil system. Neutral stability curves. Critical Rayleigh number vs dimensionless wave number α, at (a) lower liquid depths $l_1 = 0.61$ (- -), 0.62 (-.), 0.63 (line), (b) 0.64 (- -), 0.65 (-.), 0.66 (line), (c) 0.67 (- -), 0.68 (-.), 0.69 (line), (d) 0.7 (- -), 0.71 (line).

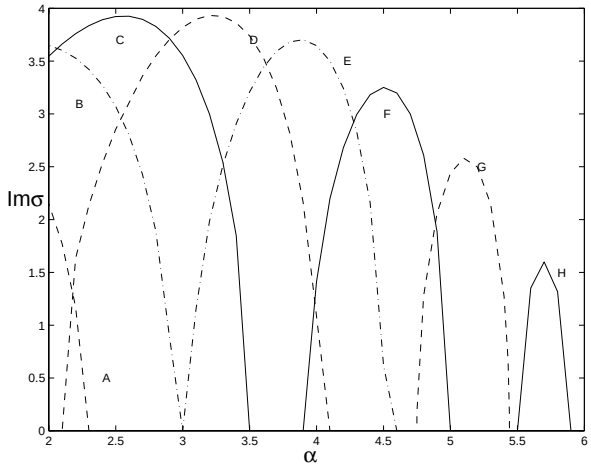

FIG. 4. Water/silicone oil system. Imσ vs dimensionless wave number α along neutral stability curves, at lower liquid depths $l_1 = 0.63$ (A), 0.64 (B), 0.65 (C), 0.66 (D), 0.67 (E), 0.68 (F), 0.69 (G), 0.7 (H).

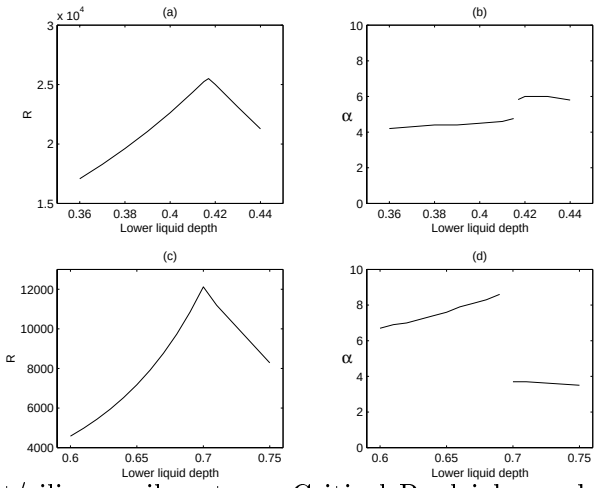

FIG. 5. (a) Fluorinert/silicone oil system. Critical Rayleigh number vs dimensionless lower liquid depth l_1. (b) Fluorinert/silicone oil system. Critical values for dimensionless wave number α vs dimensionless lower liquid depth l_1. (c) Water/silicone oil system. Critical Rayleigh number vs dimensionless lower liquid depth l_1. (d) Water/silicone oil system. Critical values for dimensionless wave number α vs dimensionless lower liquid depth l_1.

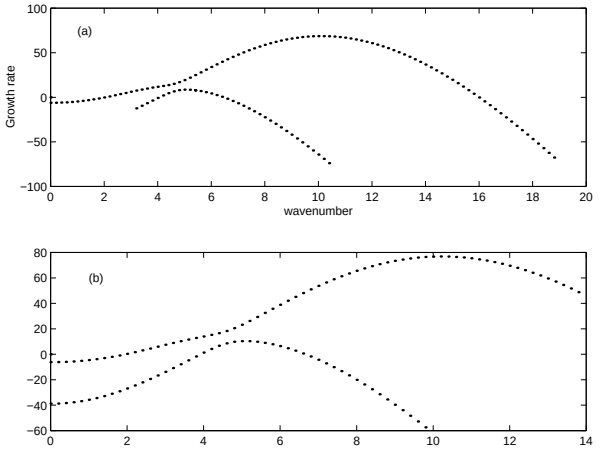

FIG. 6. Water/silicone oil system. Dimensionless growth rates Re σ of largest growing modes at (a) $R = 18,822.71$, $l_1 = 0.69$, $G = 1.043 \times 10^9$, $P = 7.1$, $\Delta T = 0.65^oC$, (b) $R = 19,733.49$, $l_1 = 0.69$, $G = 1.043 \times 10^9$, $P = 7.1$, $\Delta T = 0.65^oC$.

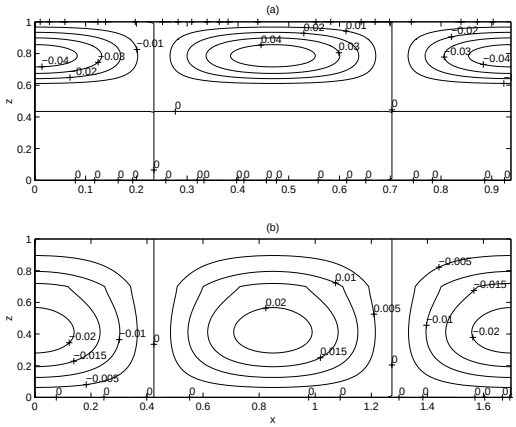

FIG. 7. Water/silicone oil system. Perturbation temperature contour plots for critical conditions of Figure 3. Steady modes. (a) Dimensionless lower liquid depth $l_1 = 0.6$, dimensionless wave number $\alpha = 6.7$. (b) $l_1 = 0.7$, wave number 3.7.

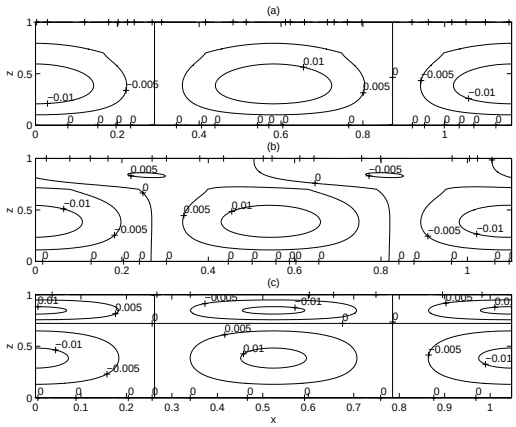

FIG. 8. Water/silicone oil system. Perturbation temperature contour plots for dimensionless lower liquid depth $l_1 = 0.7$. Oscillations occur at dimensionless wave numbers $\alpha = 5.6$ to 5.8. (a) wave number 5.4. Steady mode. (b) wave number 5.7. Oscillatory mode. (c) wave number 6. Steady mode.

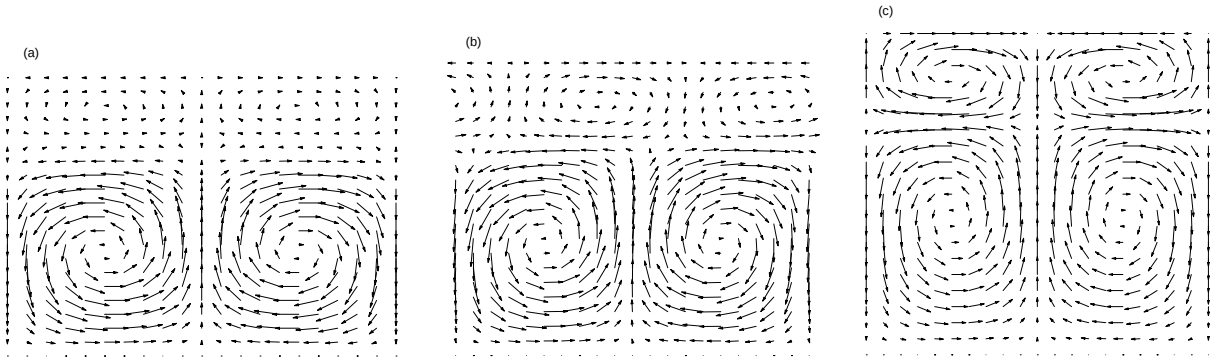

FIG. 9. Water/silicone oil system. Velocity vector plots at dimensionless lower liquid depth $l_1 = 0.69$, showing trends in the location of the rolls as the wave number passes through the Hopf range. (a) $R = 13,823$. Dimensionless wave number $\alpha = 4.5$. Rolls are thermally coupled. (b) $R = 14,205$. Wave number 5.2, inside the Hopf range. Rolls are in a transition regime. (c) $R = 12,817$. Wave number 5.9, greater than those of the Hopf range. Rolls are mechanically coupled. A summary of behavior at other depth fractions is given in Table II. The plots extend one wavelength in the x- direction, and over z=0 to 1 vertically.

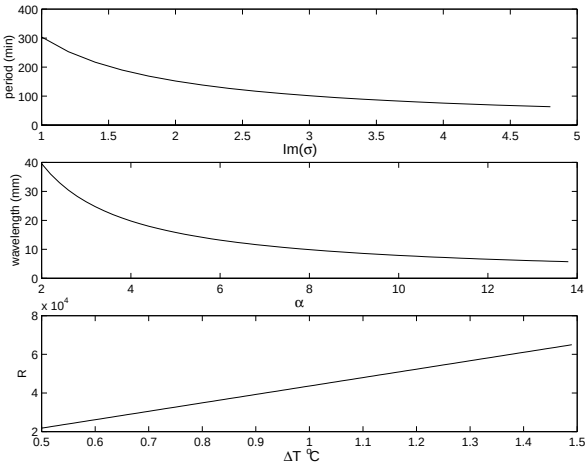

FIG. 10. Fluorinert/silicone oil 47v10 system. Dimensional period (min) vs Imσ, wavelength (mm) vs wave number α, Rayleigh number R vs perturbation temperature difference ΔT^oC. Plate separation 1.26 cm.

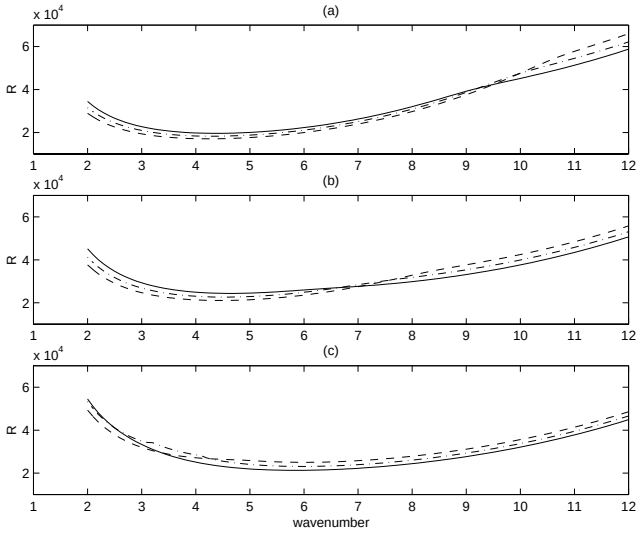

FIG. 11. Fluorinert/silicone oil 47v10 system. Neutral stability curves for the onset modes at dimensionless lower liquid depths l_1 = (a) 0.36(- -), 0.37 (-.), 0.38, (b) 0.39 (- -), 0.40 (-.), 0.41, (c) 0.42 (- -), 0.43 (-.), 0.44. Plots show critical Rayleigh number vs dimensionless wave number α.

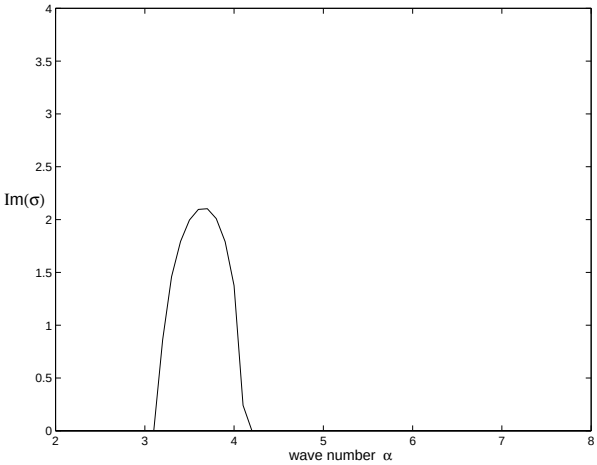

FIG. 12. Fluorinert/silicone oil 47v10 system. Imaginary part of eigenvalue σ vs dimensionless wave number α, along neutral stability curve at lower liquid depth $l_1 = 0.43$, showing oscillatory onsets. The other depths shown in Figure 11 have real onsets, not oscillatory.

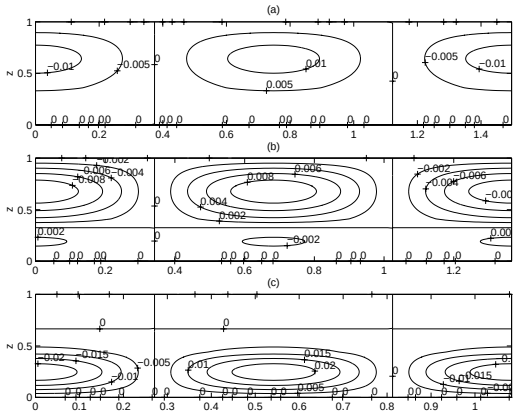

FIG. 13. Fluorinert/silicone oil system. Perturbation temperature contour plots. At each depth fraction, all wave numbers are examined to find the lowest critical value of Rayleigh numbers. Steady modes are found. (a) Dimensionless lower liquid depth $l_1 = 0.36$, dimensionless wave number $\alpha = 4.2$. (b) $l_1 = 0.41$, wave number 4.6. (c) $l_1 = 0.44$, wave number 5.8.

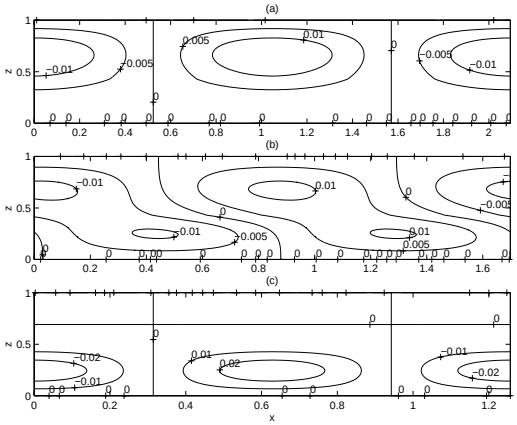

FIG. 14. Fluorinert/silicone oil system. Perturbation temperature contour plot of critical mode. Dimensionless lower liquid depth $l_1 = 0.43$. (a) steady mode at wave number $\alpha = 3.0$, slightly less than oscillatory onset shown in Figures 11 and 12. (b) wave number 3.7 at oscillatory onset shown in Figure 12. (c) steady mode at wave number 5.0, slightly more than oscillatory onset shown in Figure 12.

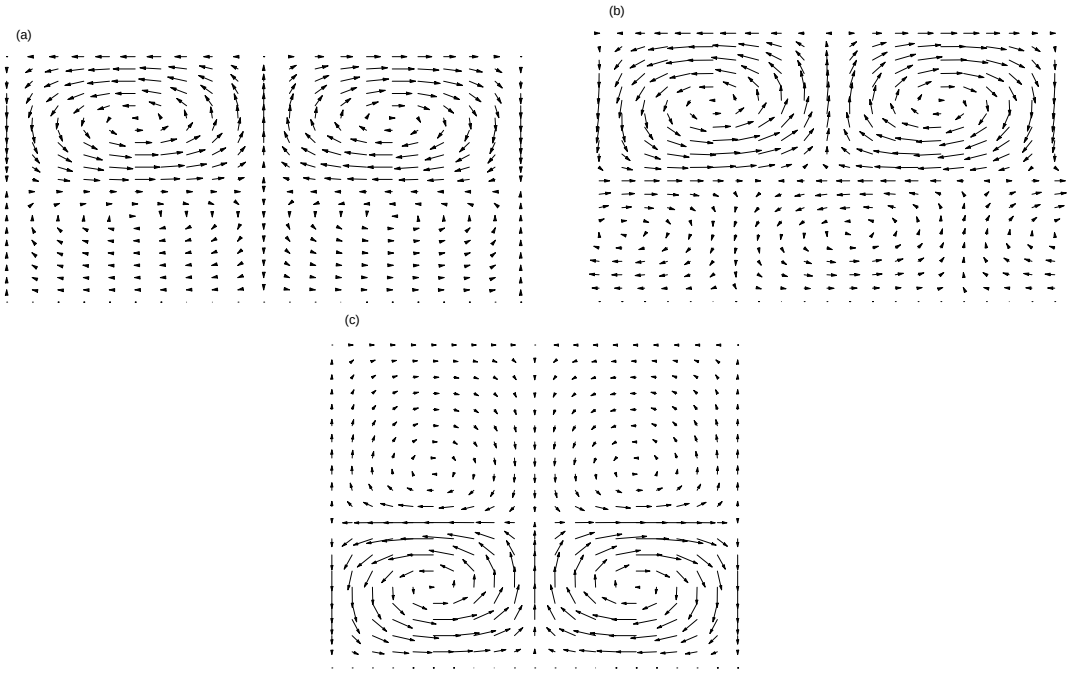

FIG. 15. Fluorinert/silicone oil system. Velocity vector plots at dimensionless lower liquid depth $l_1 = 0.43$, showing trends in the location of the rolls. (a)$R = 34,959$. Wave number $\alpha = 3.0$, less than the Hopf range. Rolls are moderately mechanically coupled. (b) $R = 30,065$. Wave number 3.7, inside the Hopf range. Rolls are in a transition regime. (c) $R = 24,044$. Wave number 5.0, greater than the Hopf range. Rolls are mechanically coupled. The plots show one wavelength in the x-direction and z extending from 0 to 1.

TABLES

TABLE I. Physical properties of 3M Fluorinert FC70, Rhone Poulenc's silicone oil Rhodorsil 47v10, Rhodorsil 47v2, and water, as given in Andereck et al (1995) and Degen et al (1998).

	CGS units	Fluorinert	47v10	47v2	water
ρ density at 25C	g cm^{-3}	1.94	.9273	0.867	0.998
ν kinematic viscosity	cm^2 s^{-1}	0.14	0.1	0.02	0.01
κ thermal diffusivity	cm^2 s^{-1}	3.45×10^{-4}	8.6×10^{-4}	$7.78 \cdot 10^{-4}$	0.00142
$\hat{\alpha}$ thermal expansion	K^{-1}	.001	1.08×10^{-3}	$1.17 \cdot 10^{-3}$	$2.067 \cdot 10^{-4}$
k thermal conductivity	g cm s^{-3} K^{-1}	7x10^3	1.3×10^4	$1.1 \cdot 10^4$	$5.98 \cdot 10^4$
surface tension with air	g/s^2	18	20.5	18.7	71.2

TABLE II. Summary of velocity vector field behavior for water/silicone oil system for depth fractions 0.65 to 0.70. Data taken at wave number less than Hopf range (thermally coupled rolls), inside the Hopf range (transition regime), and greater than Hopf range (mechanically coupled rolls). The velocity fields are illustrated in Figure 9.

l_1	α		
	thermal coupling	transition	mechanical coupling
0.62	NA	0.9	2.0
0.63	NA	1.5	2.5
0.64	NA	2.6	3.0
0.65	1.0	2.8	4.0
0.66	2.0	3.3	4.5
0.67	2.5	4.0	5.0
0.68	3.5	4.5	5.5
0.69	4.5	5.2	5.9
0.70	5.4	5.7	6.0

TABLE III. Pattern formation results for water/silicone oil system and Fluorinert/silicone oil system.

l_1	R	α	$\lvert\mathrm{Im}\ \sigma\rvert$	Stable solution
				Water-Silicone Oil System
0.62	880328	0.3	2.3	Traveling Patchwork Quilt(2)
	500657	0.4	2.2	Traveling Rolls
	226181	0.6	2.0	Traveling Rolls
	103236	0.9	1.7	Traveling Rolls
0.63	91186	1	3.2	Traveling Rolls
	43246	1.5	3	Traveling Rolls
	22823.7	2.2	1.17	Traveling Rolls
0.64	120035	0.9	3.3	Traveling Rolls and Wavy Rolls(1)
	33947	1.8	3.7	Traveling Rolls
	19184	2.6	2.8	Oscillating Triangles
0.65	74985	1.2	2.1	Traveling Patchwork Quilt(2)
	18601	2.8	3.8	Wavy Rolls(1) and Oscillating Triangles
	15237	3.3	2.5	Wavy Rolls(1) and Oscillating Triangles
0.66	26314	2.3	2.1	Traveling Patchwork Quilt(2)
	16295	3.3	3.9	Wavy Rolls(1) and Oscillating Triangles
	14146	3.8	2.8	Traveling Rolls and Wavy Rolls(1)
0.67	18008	3.2	1.98	Oscillating Triangles
	14458	4	3.6	Traveling Rolls and Wavy Rolls(1)
	13499	4.4	1.6	Oscillating Triangles
0.68	15119	4.1	2.2	Traveling Rolls
	14202	4.5	3.2	Traveling Rolls and Wavy Rolls(1)
	13728.5	4.8	2.6	Traveling Rolls and Wavy Rolls(1)
0.69	14506.8	4.9	2.06	Traveling Rolls

	14205	5.2	2.5	Traveling Rolls and Wavy Rolls(1)
	14068	5.4	1.3	Oscillating Triangles
0.70	14918	5.6	1.3	Oscillating Triangles
	14888	5.7	1.6	Oscillating Triangles
	14868	5.8	1.3	Oscillating Triangles
				Fluorinert-Silicone Oil System
0.43	30065	3.7	2.1	Traveling Rolls and Wavy Rolls(1)
	28512	4	1.4	Oscillating Triangles